Unsupervised Domain Adaptation for Gesture Identification Against Electrode Shift

Patrick P. K. Chan, *Senior Member, IEEE*, Qiuxia Li, Yinfeng Fang, *Member, IEEE*, Linyi Xu, Kairu Li, Honghai Liu, *Fellow, IEEE*, and Daniel S. Yeung, *Life Fellow, IEEE*

***Abstract*—Surface electromyogram (sEMG)-based hand gesture recognition, which interprets commands given by humans through sEMG signals, performs well in many studies. However, its recognition accuracy drops dramatically due to electrode shift since the distributions of motion classes are changed. Although calibrating the system with newly collected samples after electrode shift maintains the accuracy, collecting labeled samples is inconvenient and time-consuming since the procedure is rigid. However, the calibration may not work properly without label, especially when the change is significant. This study proposes a user friendly and convenient calibration method for hand gesture recognition by an unsupervised domain adaptation method, which only obtains the unlabeled samples of preselected benchmark classes from users in calibration. The change of benchmark classes is captured by unlabeled samples by a clustering method. The other classes are estimated based on the benchmark classes by regression models. As a result, the information of all classes is used to calibrate the system. Linear discriminant analysis is used to demonstrate our model. A dataset with ten subjects is collected to verify the performance empirically. Experimental results confirm that our method utilizes the unlabeled benchmark class samples in calibration and achieves 75.55% average accuracy. Our method is more robust to electrode shift and improves around 8.5% accuracy consistently on all subjects compared with the methods without calibration or label information in calibration. Although the accuracy of our method is slightly less than the ones using label calibration samples, our calibration data collection is more convenient and less complicated.**

Manuscript received 17 September 2021; revised 21 February 2022; accepted 2 May 2022. Date of publication 27 June 2022; date of current version 15 November 2022. This work was supported in part by the Natural Science Foundation of Guangdong Province, China under Grant 2018A030313203, and in part by the Fundamental Research Funds for the Central Universities SCUT under Grant 2018ZD32. This article was recommended by Associate Editor Vittorio Fuccella. *(Corresponding author: Patrick P. K. Chan.)*

Patrick P. K. Chan, Qiuxia Li, and Linyi Xu are with the School of Computer Science and Engineering, South China University of Technology, Guangzhou 510006, China (e-mail: patrickchan@ieee.org; liqiuxia.scut@outlook.com; czzerone@qq.com).

Yinfeng Fang is with the School of Communication Engineering, Hangzhou Dianzi University, Hangzhou 310005, China (e-mail: yinfeng.fang@hdu.edu.cn).

Kairu Li is with the School of Electrical Engineering, Shenyang University of Technology, Shenyang, Liaoning 110870, China (e-mail: kairu.li@sut.edu.cn).

Honghai Liu is with the School of Computing, University of Portsmouth, PO1 2UP Portsmouth, U.K. (e-mail: honghai.liu@icloud.com).

Daniel S. Yeung is with the IEEE Systems, Man, and Cybernetics Society, Hong Kong , China (e-mail: danyeung@ieee.org).

This work involved human subjects or animals in its research. Approval of all ethical and experimental procedures and protocols was granted by Ethics Committee of the University of Portsmouth and written informed consent was obtained from all subjects.

Color versions of one or more figures in this article are available at https://doi.org/10.1109/THMS.2022.3179956.

Digital Object Identifier 10.1109/THMS.2022.3179956

***Index Terms*—Calibration, electrode shift, gesture identification, unsupervised domain adaptation (UDA).**

I. Introduction

SURFACE electromyogram (sEMG)-based hand gesture identification is an important area of human–computer interaction. The users' commands are interpreted according to their sEMG signals. Since sEMG can be acquired easily and invasively, the sEMG-based identification has been widely used and performs well in prostheses control applications [1]–[3]. However, the experimental settings of most studies are restrictive, i.e., the electrode positions on a limb are assumed to be stationary [4]. However, in practice, the electrode positions may shift when taking off or putting on the prosthesis [5], [6], sweating [7], etc.. Since the data distributions of motions are changed by electrode shift a gesture recognition system may not predict a motion correctly. Fig. 1 shows that the mean vectors of each class shown by the two most discriminative features extracted by principal component analysis (PCA) change significantly due to the electrode shift occurred by taking off and putting on the prosthesis. Many studies [8]–[11] indicate that electrode shift dramatically reduces the accuracy of a gesture recognition system. Unfortunately, electrode shift is unavoidable because putting on and taking off a prosthesis is necessary for users. Therefore, considering nonstationary sEMG signals is important in hand gesture recognition in order to enhance its applicability.

The influence of electrode shift can be reduced by complementing redundant signals captured by the high density of electrodes [12]–[16] in *hardware-based methods*. Although these methods achieve robust performance against electrode shift, the setup and maintenance costs are high. On the other hand, most *software-based methods* calibrate the model using samples collected after electrode shift [17]–[21]. These countermeasures require collecting labeled samples for each motion class after electrode shift [17]–[20], [22] for calibration. However, users are required to carefully perform the motions of every motion class in a specific and rigid order, during which any small mistake may cause the process start over again. Because of these restrictions, recalibration is usually time-consuming and inconvenient for users. To make matters even worse, electrode shift may happen several times a day. On the other hand, the self-enhancing (SE) method [21] is adjusted according to its predicted labels, which means it heavily relies on the accuracy of its prediction and, thus, performs badly when the change caused by electrode shift is significant [23].

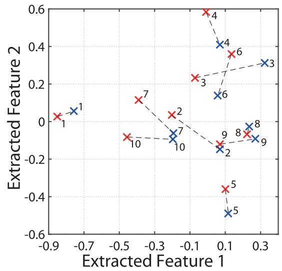

Fig. 1. Illustration on the influence of electrode shift on the data distributions. Samples of a subject are collected from different 2 d shown in different colors. A cross denotes a mean vector of each class represented by the two most discriminative features extracted by PCA. A dashed line represents a change of the mean of a class.

By this observation, our study aims to investigate a calibration method that offers a more convenient data collection process. A user is only required to perform a subset of motions that have been preselected in an arbitrary order for the data collection. The parameters of all motion classes are then estimated to calibrate the gesture recognition system. As a result, the data collection process of our proposed method is more convenient, more user friendly, and less time-consuming than existing ones, which require to collect labeled samples of all motion classes under rigid instructions. Moreover, the performance of our method should be more stable and accurate than the SE methods and the ones without calibration since our method is not completely reliant on the gesture recognition system itself.

An unsupervised domain adaptation (DA) method for sEMG-based hand gesture recognition using linear discriminant analysis (LDA) is devised in this article. This method estimates the label information used in calibration according to the characteristics of samples. After electrode shift, samples of the preselected motion classes are collected in an arbitrary order. The collected samples are first separated into the preselected classes by using a cluster method, and then, the distribution parameters of other classes are estimated by regression based on the information of the preselected classes. The gesture recognition system is then calibrated with this estimated information. LDA [24], [25] is focused in this study due to its satisfying performance, low complexity, and practicality in sEMG-based hand gesture recognition. Our proposed method is compared with the existing DA methods using LDA as a classifier empirically using our collected dataset containing ten motions from ten intact-limbed subjects for 10 d. The experimental results confirm our expectation that with limited effort from users required during data collection, the proposed method provides useful information for calibration.

The rest of this article is organized as follows. The related concepts of our study are briefly introduced in Section II. Section III devises and discusses our proposed model in detail. The experimental results and discussion are given in Section IV. The conclusion is given and the future work is discussed in Section V.

II. Background

The current software-based countermeasures against electrode shift mainly focus on LDA, which is a promising classifier with satisfying results in sEMG-based gesture recognition. Those methods aim to estimate or update the means (μ) and covariances (Σ) of classes after electrode shift in order to reduce its influence.

TABLE I
Summary of the Latest Software-Based Countermeasures Against Electrode Shift

Method	Offine Calibration	Online Calibration
gCMCA [23]	/	/
SE [21]	/	Unlabelled sample
CA [20]	Labelled samples of all motions	Unlabelled sample
DA [18]	Labelled samples of all motions	/

No calibration is carried out in the global common model component analysis (gCMCA) [23], which assumes samples of the same motions contain some characteristics that are robust to electrode shift. Dissimilarity (L) is defined to measure the divergence of a model affected by different electrode shifts for every class by using KL-divergence. All samples are projected to the space with the minimum KL-divergence for recognition, and no calibration is needed. However, gCMCA may not work well when the change caused by electrode shift is significant, since the samples affected by different electrode shifts may differ considerably with others.

The SE method [21] updates the system online by using a test sample and its predicted label. As a result, no calibration set is required. For each test sample with a predicted class, the updated μ and Σ of the predicted class in LDA are calculated according to the old μ and Σ. Advantages of SE are that no additional calibration and no label information are required. However, similar to gCMCA, SE performs well for slight electrode shift only when the data distribution does not change dramatically. When the samples are very different from the ones before electrode shift, the calibration may be misled by inaccurately predicted labels.

Most countermeasures calibrate the gesture recognition system using newly collected samples after electrode shift. Cascaded adaptation (CA) [20] will be self-enhanced online by updating the parameters of LDA according to μ and Σ of the new labeled samples collected after electrode shift. DA [18] is another method requiring a calibration set with label information. Base systems are first trained on the data acquired from different prior days. When electrode shift occurs, the reusability degree of a model is measured by the Mahalanobis distance from the new model to the old model for the class. μ and Σ of the final model are calculated by the weighted means and covariances of base models according to the revised degrees and also μ and Σ of the newly collected samples. As the complete set of labeled samples provides rich and useful information on the new distribution, DA and CA achieve satisfactory performance. However, collecting labeled samples is inconvenient and time-consuming for users. The aforementioned software-based countermeasures against electrode shift are summarized in Table I.

Recently, some unsupervised DA methods are proposed for hand gesture calibration. However, these studies either focus on high-density EMG [15], [16], which uses much more signals in order to reduce the influence of electrode shift, or use deep learning [22] which suffers from high time complexity.

III. Proposed Unsupervised DA Method

The performance of gesture recognition decreases with electrode shift because of the change of the data distribution. Most calibration methods require labeled samples of all motions to address domain discrepancy. Not only is a user required to follow the complicated procedure carefully in data collection, in some cases, an additional device may be required. These methods are time-consuming and inconvenient, especially electrode shift may happen several times a day. However, calibration without label information may be unstable and inaccurate, and is only suitable for slight electrode shift. This section devises an unsupervised DA method for gesture identification against electrode shift, which aims at reducing the user effort in data collection after electrode shift. Only unlabeled samples of a few selected motion classes are required, and the order of performing these motions is irrelevant in data collection. The data distribution changed by electrode shift is estimated according to the preselected classes. Thus, the data collection of our method is much simpler and user friendly than ones collecting labeled samples of all classes.

LDA is focused on in our proposed unsupervised DA method due to its simplicity, popularity, and efficacy in hand gesture recognition. It aims to classify a sample $\mathbf{x} \in D^{te}$ into $y \in C = \{1, 2, \ldots, c\}$, where $\mathbf{x}$ is a feature vector, and c is the number of classes representing hand gestures. We assume k datasets D_i^{tr} are collected from the same person after different electrode shifts for training, where $i = 1, 2, \ldots, k$. The data distributions of any D_i^{tr} as well as D^{te} are different due to the influence of different electrode shifts.

Benchmark classes are selected from motion classes according to the isolation and stability in advance, as described in Section III-B. After electrode shift, a user is required to perform preselected motions, called benchmark classes (B), in an arbitrary order. As a result, a dataset (D^b) containing unlabeled samples of the benchmark motion classes is collected, and follows the same distribution of D^{te}. The unlabeled samples are separated into clusters by k-means, and each benchmark class represented by a cluster is then identified. The parameters of the data distribution of each benchmark class are calculated. Next, the parameters of the rest of the classes are estimated according to the benchmark classes (see Section III-C). Finally, the LDA classifiers are calibrated according to the estimated parameters. Details of the proposed unsupervised DA are described in Section III-D. The proposed model is illustrated in Fig. 2.

A. Data Acquisition and Processing

A dataset is collected to verify and illustrate our method. In total, ten able-bodied subjects with an age range of 22–31 from the University of Portsmouth, U.K., volunteered for the experiment. The gender is not considered since it is irrelevant to the experimental results. The subjects were all normally limbed with no neurological or muscular disorders.

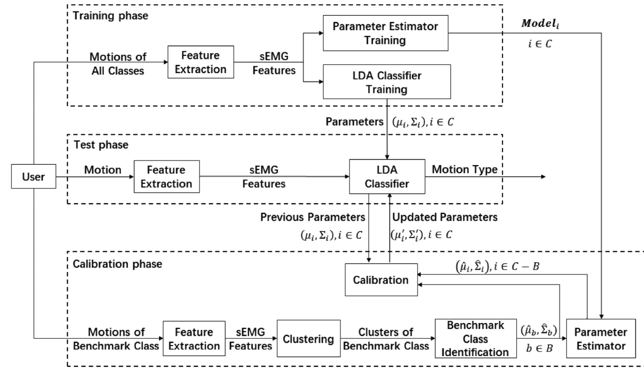

Fig. 2. Data flowchart of the training, calibration, and test phases of the proposed method.

Fig. 3. Experimental setup for sEMG data collection.

The sEMG acquisition system [26] used in the data acquisition is customized by the Intelligent System and Biomedical Robotics Group of University of Portsmouth, as displayed in Fig. 3. The system mainly consisted of following three components as described in [26] and [27]:

1) an electrode sleeve,
2) a 16-channel sEMG signal amplifier,
3) signal acquisition software (3).

The electrode sleeve which was designed to embed 18 dry electrodes on flexible fabric, forming 16 bipolar sEMG channels is put on the forearm of the volunteer to collect data. The electrodes are evenly distributed on the electrode sleeve, which ensures the high quality of electrode signal collection. An empty sleeve was employed to cover the electrode sleeve to mitigate movement artifacts. The sEMG signal was enhanced by the amplifier with a gain of 1000 and a sampling rate of 1000 Hz. For the captured EMG signals, the lowest resolution is 5.72 μV with 12 bits sampling resolution. In addition, the amplifier also depressed the frequent components beyond the range of 20–500 Hz and 50 Hz (power line noise frequency) for each individual sEMG channel. The sEMG signal acquisition software was developed to synchronize, record, and process the sEMG signal in a visual manner. Each motion data has 16 channel EMG segments with a duration of 10 s, and the data are artifact free by removing low-frequency artifacts.

In the experimental protocol [18], [21], all subjects were asked to place the electrodes with a rough reference (i.e., two ground electrodes placed on the ventral side of the forearm and the sleeve pulled right above the elbow) without the use of electrode location markers. After wearing the sleeve, the procedure was

TABLE II
THE TEN HAND MOTIONS IN OUR COLLECTED DATASET

Motion Id	Motion Name	Motion Image	Motion Id	Motion Name	Motion Image
M1	Hand Rest		M6	Wrist Pronation	
M2	Hand Open		M7	Wrist Supination	
M3	Hand Closed		M8	Ulnar Flexion	
M4	Wrist Flexion		M9	Radial Flexion	
M5	Wrist Extension		M10	Fine Pinch	

introduced to the subjects in a face-to-face teaching manner on the first acquisition day. During data capturing, subjects sat comfortably in an office chair and put the right elbow on the desktop. There was no restricted rule on the elbow joint angle or the force effort on the gestures. Each subject was required to implement two sessions each day with an interval of about half an hour. For each session, subjects were required to follow the cue signals shown on a screen to perform hand motions sequentially in an arbitrary order, and each motion lasted for 10 s under the supervision to ensure accuracy and effectiveness. Each motion is performed once in each session but repeated in different sessions. Since our research focuses on static motion, the motion speed is beyond our consideration and is removed. The data of ten motions, listed in Table II, are collected from ten subjects for 10 d.

Feature extraction is performed on the collected sEMG data. The sEMG data are segmented using a series of 300 ms analysis windows and 50 ms window shifts. A 50 ms window shift is sufficient for real-time requirements. A sample is defined as root-mean-square features of the sEMG data within a window due to its simplicity and excellent performance in hand gesture recognition [28]. As a result, (10 000 − 300)/50 + 1 = 195 samples are extracted for each motion in a session. To obtain the steady-state samples, only 155 samples in the middle are used. Therefore, 3100 samples (310 samples for each motion) of a subject are extracted each day, and each sample is a 16-D vector due to 16 channels in our dataset.

B. Benchmark Class Selection

As the distribution of the rest of the classes are estimated based on the benchmark classes, benchmark classes' selection is a critical factor in our proposed method. The parameters of the benchmark classes are estimated according to the unlabeled samples in an arbitrary order during calibration data collection. Therefore, the benchmark classes should be isolated and stable in order to increase the accuracy of the benchmark class identification.

A set of benchmark classes (B) should be selected in advance by investigating the motion classes using the k training sets, i.e., D_i^{tr} where $i = 1, 2, \ldots, k$. Two measurements are proposed to quantify the *isolation* and *stability* of a pair of motion classes. As no label information is obtained, it is preferable that samples from different benchmark classes are distinguished. *Isolation* ($\text{Iso}_{(i,j)}$) of classes i and j is defined as the average ratio of intercluster distances and intracluster distances between a class

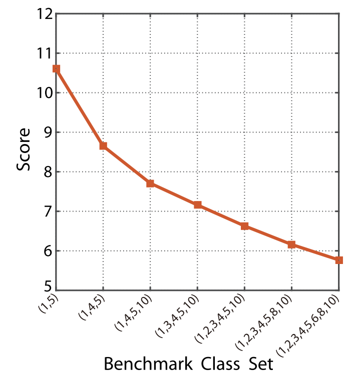

Fig. 4. Benchmark class set with size $= 2, 3, \ldots, 8$ in our collected dataset.

pair among all training sets

$$\text{Iso}_{(i,j)} = \frac{\sum_{r=1}^{k} d(\mu_i^r, \mu_j^r)}{\sum_{t=1}^{k} (\Sigma_i^t + \Sigma_j^t)} \tag{1}$$

where μ_i^r and Σ_i^t denote the mean and standard deviation of the ith class in D_r^{tr} and D_t^{tr}, respectively, and $d(\mu_i^r, \mu_j^r)$ represents the Euclidean distance between μ_i^r and μ_j^r. A pair of classes with a larger Iso indicates they have larger intercluster distances and less intracluster distances, which can be separated more easily. As a result, a larger Iso is more preferable. After the samples are separated into different clusters, the motion class represented by each cluster should be identified. Stability ($\text{Sta}_{(i,j)}$) of classes i and j measures the average change of angle between classes i and j on D_i^{tr}, where $i = 1, 2, \ldots, k$, defined as

$$\text{Sta}_{(i,j)} = \frac{1}{\binom{k}{2}} \sum_{\substack{r,t=1 \\ r \neq t}}^{k} \arccos\left(\frac{v_{i,j}^r \cdot v_{i,j}^t}{\| v_{i,j}^r \| \| v_{i,j}^t \|}\right) \tag{2}$$

where $v_{i,j}^r$ denotes the vector between the means of the ith and jth classes in D_r^{tr}, and $\binom{a}{b}$ denotes the combination of b elements from a elements. A small change in the relative locations is expected when Sta is small.

For a given set T, score(T) is defined as

$$\text{score}(T) = \frac{2}{|T|(|T|-1)} \sum_{\substack{i,j \in T \\ i<j}} \left(\text{Iso}_{(i,j)} + \frac{1}{\text{Sta}_{(i,j)}}\right) \tag{3}$$

where $|T|$ denotes the cardinality of T. A set with a larger $\text{Iso}_{(i,j)}$ and lower $\text{Sta}_{(i,j)}$ is more preferable. As a result, the selection of b benchmark classes from the set of all motion classes (C) is formulated as an optimization problem maximizing score

$$B = \arg\max_{T \subseteq C} \text{score}(T), \quad \text{s.t.} |T| = b. \tag{4}$$

The dataset we collected is used as an example to illustrate the concept of the benchmark class selection. All samples of the ten classes are used to calculate Iso and Sta in this discussion.

The best combinations of motion classes with the size $= 2, 3, \ldots, 8$ and their scores of (4) are listed in Fig. 4. The figure indicates that the selection of the benchmark classes is stable, i.e., $B_a \subset B_b$, where B_a denotes the set containing a number

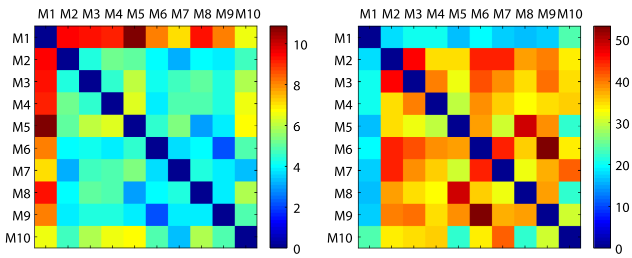

(a) (b)

Fig. 5. Isolation and stability measure of all class pairs in our collected dataset. (a) Isolation measure. (b) Stability measure.

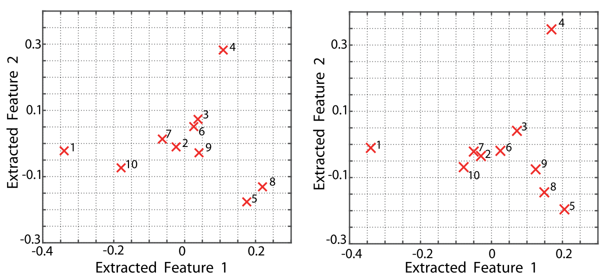

(a) (b)

Fig. 6. Illustration on the first two components of the means vectors of all motion classes of subject 3 extracted by PCA. (a) Day 1 training set. (b) Day 3 training set.

of benchmark classes, and $b > a$. Hand rest ($M1$) and Wrist extension ($M5$) classes are the most suitable for benchmark classes as they are chosen in all cases. The score of B with more classes is smaller since classes will overlap with others more easily. However, a smaller B may not provide sufficient information to estimate the distribution information of other classes.

Fig. 5 shows Iso and Sta for all class pairs. The ith row represents the measure between Mi to other classes. Colors of each grid represent different values. As both measures are a symmetric function, the tables are also symmetric. Iso values between $M1$ and other classes are larger than six. As $M1$ represents the hand rest motion, all muscles are relaxed at this stage, which is significantly different from other motions. It explains why $M1$ is the most isolated from others. Also because of this muscle relaxation, $M1$ is most stable in terms of the change of angles shown in Fig. 5(b), i.e., its Sta values are the smallest among all the classes. Wrist flexion ($M4$) and wrist extension ($M5$) also obtain large Iso and small Sta values compared with other classes, because both motions require the movement of the large arm muscle.

The distributions of the motion classes in our collected dataset are illustrated visually in Fig. 6. *X*-axis and *y*-axis are the two most discriminative features of the mean vectors of all classes of the samples of subject 3 collected in day 1 and day 3, as extracted by PCA, and a cross denotes the mean of a class. As $M1$, $M4$, and $M5$ are easily discriminated from other classes, they are chosen as the benchmark classes with different sizes in previous discussion. $M8$ is not considered although $M5$ and $M8$ are close to each other. This is because $M8$ is also closer to other classes and is less stable than $M5$. For example, $M8$ is located on the left- and right-hand sides of $M4$ in day 1 and day 3. The quantification measures also indicate that the subset $\{M1, M4, M5\}$ is more preferable as a benchmark since score $\{M1, M4, M5\}$ and score $\{M1, M4, M8\}$ are 26.50 and 23.34, respectively. To be specific, the average Iso and Sta of $\{M1, M4, M5\}$ are 8.78 and 21.96, while $\{M1, M4, M8\}$ are 7.73 and 22.80. Therefore, $\{M1, M4, M5\}$ is more stable and isolated than $\{M1, M4, M8\}$. The figures provide another point of view to verify the correctness of our proposed selection method on benchmark classes.

C. Parameter Estimator for Nonbenchmark Class

The parameter estimator aims to estimate the parameters of a nonbenchmark class according to the parameters of benchmark classes. We assume that k datasets D_i^{tr} collected from the same person after different electrode shifts are obtained. For each D_i^{tr}, the mean ($\hat{\mu}_j$) of samples in the jth class in each window with the size n and stride d is calculated. Those mean vectors generate the training set for the parameter estimator for the rth nonbenchmark class $D_r = \{\mathbf{x}, \mathbf{y}_r\}$, where $\mathbf{x} = \{\hat{\mu}_b | b \in B\}$, $\mathbf{y}_r = \hat{\mu}_r$, and $r \in (C - B)$.

In our study, the random forest (RF) with the CART decision tree algorithm [29] is chosen as a regression model for the parameter estimator since RF achieves good performance on a complex and nonlinear problem with a small training set [30]. $|\mathbf{y}_i|$ RF model is trained for each nonbenchmark class.

D. Proposed Unsupervised DA

A set of unlabeled samples of the benchmark class (D^b) is collected after electrode shift. K-means clustering is applied to assign the samples into b clusters. Centers of b clusters are assigned randomly at the beginning, and then are updated by the mean of the samples of a cluster iteratively.

As discussed in the previous section, the benchmark classes are stable and isolated. The benchmark class represented by a cluster is identified according to the relative position of the clusters. To be more specific, in order to reduce the complexity of identification, the mean vectors of benchmark classes of samples in the training set are first projected into a 2-D space composed of the two most informative features extracted by PCA. $M4$ is the cluster that has the mean with the largest value of extracted feature 2 (i.e., the cluster on the top in Fig. 6). The rest of the clusters are identified as $M1$ and $M5$ according to the value of extracted feature 1, i.e., the mean with a smaller (bigger) value is $M1$ ($M5$), since the cluster is located on the left-hand side (right) in Fig. 6. Finally, the distribution parameters including mean $\hat{\mu}_b$ and covariance $\hat{\Sigma}_b$ are calculated using the samples of a cluster for each benchmark class, where $b \in B$.

Similar to the previous studies [17], [21] in which the classes are homoscedastic when using LDA in gesture identification is assumed initially, our model also assumes that Σ of all classes is the same, and mainly focuses on μ. The estimated $\hat{\mu}_b$ is fed into the trained parameter estimators, defined in Section III-C, to calculate $\hat{\mu}_i$ for each nonbenchmark class, where $i \in (C - B)$.

Algorithm 1: Unsupervised DA Algorithm.

Input: g_i: Parameter Estimator, $i \in C$;
D^b: Set of unlabeled benchmark class samples;
C: Set of all motion classes
B: Set of benchmark motion classes;
μ_i, Σ_i: Parameters of current LDA, $i \in C$
$G_b = \text{Kmeans}(D^b, b)$ // cluster unlabeled data
$C_b = \text{GetLabel}(G_b)$ // identify benchmark classes
$\hat{\mu}_b, \hat{\Sigma}_b = \text{GetPar}((D^b, C_b)$ // calculate parameters
for each $i \in C - B$ **do**
  $\hat{\mu}_i = g_i(\{\hat{\mu}_b | b \in B\})$ // estimate mean for class i
end for
$\hat{\Sigma} = E_{b\in B}[\hat{\Sigma}_b]$ // estimate variance
for each $i \in C$ **do**
  $\mu_i', \Sigma_i' = \text{Update}(\mu_i, \Sigma_i, \hat{\mu}_i, \hat{\Sigma}_i)$ // Update LDA
end for
Output: Updated LDA, $\mu_i', \Sigma_i', i \in C$;

$\hat{\Sigma}$ is calculated by averaging all $\hat{\Sigma}_b$. LDA of each class in the model is then updated by using its estimated $\hat{\mu}$ and $\hat{\Sigma}$ according to (5). The procedures of our proposed unsupervised DA is shown in Algorithm 1.

$$\mu_i' = r\mu_i + (1-r)\hat{\mu}_i, \quad \Sigma_i' = r\Sigma_i + (1-r)\hat{\Sigma}_i. \tag{5}$$

E. Computational Complexity

In addition to the LDAs, the parameter estimators, which are regression method, should also be trained in the training phase. Therefore, the time complexity of the training is in $O(n_{Tr} + n_{\text{non}B} \times j)$, where n_{Tr} represents the size of the training set, $n_{\text{non}B}$ represents the number of nonbenchmark motion samples, and j denotes the learning iteration number of the regression method. On the other hand, the time complexity for the calibration of our method is in $O(n_{\text{Ca}-B} \times i)$, where $n_{\text{Ca}-B}$ represents the number of benchmark motion samples in the calibration set, and i denotes the learning iteration number of the clustering method.

IV. Experiment

This section aims to evaluate the proposed method and compare it with existing LDA-based hand gesture recognition methods against electrode shift experimentally.

A. Experimental Setting

For each subject, 3100 samples are collected for each of 10 d. In total, 9 out of the 10 d are randomly selected as the training set (3100 × 9 = 27 900), and the rest of samples (3100) is reserved for recalibration (1400) and evaluation (1700). A classifier is trained only based on the training set, and the test samples are not presented until evaluation. Classification is performed individually for each subject, and an independent classifier is implemented for each subject. The performance of a method is evaluated according to the average accuracy achieved in tenfold cross-validation. The accuracy of classification is used to evaluate the performance.

TABLE III
Influence of Electrode Shift on the Motion Classes

$M1$	$M2$	$M3$	$M4$	$M5$	$M6$	$M7$	$M8$	$M9$	$M10$
0.041	0.111	0.148	0.183	0.214	0.167	0.098	0.205	0.169	0.092

TABLE IV
Influence of Electrode Shift on the Subjects

$S1$	$S2$	$S3$	$S4$	$S5$	$S6$	$S7$	$S8$	$S9$	$S10$
0.215	0.126	0.102	0.235	0.199	0.228	0.137	0.027	0.085	0.072

The proposed method is compared with five popular LDA-based gesture identification methods experimentally: *standard classifier (base)* in which no mechanism for electrode shift is used serves as the base for comparison, *gCMCA,* which is *CMCA* with *global* optimization [23], *SE method* [21], *CA* [20], and *DA* [18]. After electrode shift, CA and DA need to obtain the label information from a user for calibration, while SE only calibrates using the unlabeled test samples. *base* and gCMCA do not update the classifier.

Preliminary experiments have been carried out to determine suitable values for the parameters of each method, aiming to maximize the accuracy of gesture recognition. For our method, the evaluated value of tradeoff ω is set as 0.2 and 0.5, respectively. For CA and DA, the value of tradeoff ω are 0.6 and 0.6. The dimensionality of the common model component d for gCMCA is set to 15, which is suggested by a previous study [23]. The numbers of training, recalibration, and test samples are 2790, 50, and 170, respectively, for each class. All experiments are performed on a desktop PC with a 4-core 3.10 GHz CPU, 12 GB memory, and 64-bit Windows 10. All methods are implemented in a 64-bit MATLAB 2014a.

B. Analysis on Electrode Shift Influence

The influence of electrode shift on the motion classes is analyzed in this section. The influence is defined as the average difference of the mean of a motion class caused by different electrode shifts. The influence of a motion class and a subject are shown in Tables III and IV.

In general, $M1$ and $M10$ are less sensitive to electrode shift (i.e., the average difference is 0.041 and 0.092, respectively), while the average changes of $M5$ and $M8$ are 0.214 and 0.205, respectively, which are the largest among all the classes. Although the changes of $M4$ and $M5$ are relatively large, they are chosen as the benchmark classes when $b \leq 3$, as shown in Section III-B. This is because they are located far away from other classes and the data fluctuation does not increase the difficulty of identification.

Because EMG signals generated by different muscles are influenced differently by electrode shift, the sEMG signals from superficial muscles are relatively more sensitive to electrode shift compared with deep muscles. As a result, an activity using deep muscles is not closely related to the accurate positions of

TABLE V
AVERAGE ACCURACY (%) OF ALL METHODS ON EACH SUBJECT

Subjects	No Calibration		Calibration w/ label info.		Calibration w/o label info.		Mean
	base	*gCMCA*	*CA*	*DA*	*SE*	Our method	
S1	**61.53**	**61.02**	74.77	**82.30**	**61.01**	71.98	68.77
S2	**65.35**	**64.49**	**82.34**	**84.58**	**65.61**	75.13	72.92
S3	**78.60**	**77.59**	86.54	86.60	**78.64**	86.39	82.39
S4	**61.36**	**60.42**	**87.38**	**89.21**	**61.22**	71.58	71.86
S5	**76.15**	**76.19**	82.52	**90.83**	**76.65**	84.86	81.20
S6	**64.81**	**63.00**	**91.09**	**93.88**	**64.96**	78.09	75.97
S7	71.70	**71.64**	**95.31**	**92.35**	71.16	79.01	80.19
S8	61.29	60.47	**88.34**	**91.47**	62.08	66.32	71.66
S9	**61.23**	**60.92**	**88.28**	**86.09**	**61.38**	68.00	71.00
S10	**69.26**	**66.29**	**91.69**	**90.29**	**69.06**	74.19	76.79
Mean	**67.13**	**66.20**	**86.84**	**88.76**	**67.18**	75.55	75.28
Std. Dev.	6.50	6.61	5.80	3.72	6.51	6.63	

Note: The bold values indicate 95% statistically significant difference between the performance of the method and our proposed method.

TABLE VI
AVERAGE ACCURACY (%) OF ALL METHODS FOR EACH CLASS

Classes	No Calibration		Calibration w/ label info.		Calibration w/o label info.		Mean
	base	*gCMCA*	*CA*	*DA*	*SE*	Our method	
$M1\star$	**93.55**	**92.78**	99.13	98.64	**93.34**	98.87	96.05
$M2$	64.62	62.44	**90.55**	**92.80**	65.04	65.26	73.45
$M3$	**69.86**	**70.32**	**88.73**	**92.62**	**70.23**	79.81	78.59
$M4\star$	**65.57**	**64.04**	**91.26**	**87.71**	**66.22**	77.75	75.42
$M5\star$	**64.28**	**66.16**	88.76	87.76	**64.62**	85.38	76.16
$M6$	**49.39**	**49.87**	**74.88**	**80.45**	**50.35**	57.35	60.38
$M7$	70.05	**67.98**	**89.20**	**87.70**	69.73	72.70	76.23
$M8$	**58.24**	**55.77**	75.59	82.44	**58.09**	76.10	67.71
$M9$	**59.84**	**58.61**	**80.42**	**83.35**	**58.74**	69.05	68.33
$M10$	**75.89**	74.06	**94.16**	**95.53**	75.49	71.19	81.05

$\star$ A benchmark class.
Note: The bold values indicate 95% statistically significant difference on the performance of the method compared with our proposed method.

electrodes. This explains why $M2$ and $M9$ are influenced more severely by electrode shift than $M10$.

In addition, the collected dataset also indicates that the influence of electrode shift is subject dependent. $S8$, $S9$, and $S10$ are more robust to electrode shift, i.e., the changes of their samples are less than other subjects. On the other hand, $S1$, $S4$, and $S6$ suffer from electrode shift seriously, i.e., their average differences are 0.215, 0.235, and 0.228, respectively.

C. Experimental Results

The performance of the five methods is first evaluated in terms of accuracy in Section IV-C1. Section IV-C2 analyzes how a training set and a calibration set affect the performance, respectively. The running time of the training, calibration, and test phases of the methods is shown in Section IV-C3.

1) Performance Evaluation: Performance of *base*, gCMCA, DA, CA, SE, and our method in terms of classification accuracy on a subject and motion is shown in Tables V and VI, respectively. A value is calculated as the mean of all accuracy values on the test sets in te-fold cross-validation. A bold value indicates 95% statistically significant difference in the performance of our method and another method according to their *P*-values.

Table V suggests that calibration using complete information, i.e., the labeled samples collected after electrode shift, plays an important role in gesture identification. The average accuracy of the methods with calibration using label information (DA and CA) is 86.84% and 88.76%, which are significantly higher than all other methods, especially compared with *base*, gCMCA, and SE. For example, the accuracy values of DA and CA are at least 26% higher than *base*, gCMCA, and SE in $S4$, $S6$ and $S8$. Moreover, the performance of the methods requiring labeled samples is more stable than others. This is because labeled samples provide more accurate information on the new data distribution, i.e., this hand gesture recognition can be consistently good. DA is more stable and accurate than CA. As the model is updated online continuously by the SE method in CA, the model may be misled by wrongly classified samples.

Our method performs consistently better than *base*, gCMCA, and SE on all subjects, i.e., our accuracy is 8.42%, 9.35%, and 8.37% higher on average, respectively. These results confirm that the distribution information estimated by our proposed method is useful for calibration, and more informative than the predicted labels used by SE. Our method is less accurate than CA and DA as expected since no label information is provided in our method. The accuracy of our method is sacrificed to gain the convenience in data collection, i.e., no label information and only samples of the preselected motions are required in no particular order. The performance of our method relies on the estimation accuracy of the class parameters. However, the estimation accuracy is subject dependent, i.e., the performance of our method is slightly less stable than others. For example, the performance of our method is close to DA and CA for $S3$ and $S5$ (less than 6% difference), while there is around 25% difference for $S8$.

The previous study [21] shows that SE performs well for slight electrode shift, which is different from our experimental results, i.e., SE shows nearly no improvement in comparison with *base*. This is because the cross-day data are used in our experiment and its distribution may change dramatically. Inaccurate predictions downgrade the quality of calibration of SE. These classification errors may also explain why the average accuracy of SE is nearly as low as *base*. For methods without calibration, gCMCA does not show any superiority compared with *base*, which contradicts the findings in the previous study [23]. One reason may be that the dimensionality of our samples is much lower than the ones used in [23]. gCMCA cannot find common characteristics of the datasets contaminated by different electrode shifts efficiently.

Table VI tabulates the accuracy of the methods in recognizing each motion class. Identifying $M1$ and $M10$ is generally the most accurate (i.e., the average accuracy is 96.05% and 81.05%, respectively) among all classes since the classes are less sensitive

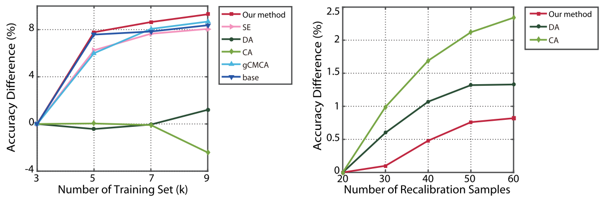

(a) (b)

Fig. 7. Accuracy difference between the methods using different numbers of training sets (k) and sizes of the calibration set (u). (a) k. (b) u.

to electrode shift, i.e., the change of their means due to electrode shift is small, as shown in Table III. On the other hand, since $M6$, $M8$, and $M9$ change significantly, only 60.38%, 67.71%, and 68.33% average accuracies are achieved, which are less than other classes, especially for the methods without collecting labeled samples after electrode shift.

Accuracy on $M1$, $M4$, and $M5$, which are used as benchmark classes, is generally higher than the ones of a nonbenchmark class in our method, since the distribution parameters of benchmark classes are directly calculated by using the unlabeled samples. The performance of our method is better than *base*, gCMCA, and SE, but generally worse than DA and CA. These results are consistent with our expectation that labeled calibration samples benefit to gesture recognition but also cause inconvenience to users. Our method extracts useful information from unlabeled calibration data, which significantly simplifies the process of data collection. For nonbenchmark classes, although the performance of our method on $M10$ is the worst among all methods, the accuracy of our method on $M3$, $M6$, $M8$, and $M9$ is significantly larger than *base*, gCMCA, and SE.

The experimental results indicate that the accuracy and stability of our method are consistently higher than *base* and gCMCA, which involve no calibration after electrode shift. Methods requiring labeled samples (i.e., CA and DA) generally perform better than our proposed method. However, when the influence of electrode shift on the data distribution is small, the accuracy of our method is close to, and sometimes even better than CA and DA. These results confirm that using unlabeled samples in the calibration phase enhances the robustness of gesture recognition to electrode shift.

2) Influence of Training Data Knowledge and Calibration Data Knowledge: The influence of the number of training sets (k) and the size of the calibration set (u) on the methods is evaluated and their results are shown in Fig. 7(a) and (b), respectively. The x-axis represents k and u, while the y-axis shows the difference between the accuracy of models with different k and u, and the base model. The base models use $k = 3$ and $u = 20$, respectively.

The number of training samples has less influence on DA and CA than other methods as their performance is less fluctuated. This is because they are calibrated by using labeled samples, which provide rich labeled information for updates. However, the performance of *base*, gCMCA, SE, and our method relies on the training sets since only partial or no information is obtained in calibration. The improvement rates on *base*, gCMCA, SE, and our method reduce with the increase of k since the difference among training sets may be smaller when k is large. Moreover, since additional information benefits the distribution parameters estimation in our model, using more training sets affected by different electrode shifts improves the performance of our method more than other methods.

TABLE VII
RUNNING TIME (IN SECOND) OF THE TRAINING, CALIBRATION, AND TEST PHASE OF THE METHODS ON DIFFERENT SIZES OF DATASETS

	Dataset Size	No Calibration		Calibration w/ label info.		Calibration w/o label info.	
		base	*gCMCA*	*CA*	*DA*	*SE*	Our method
Training Phase	x1	0.16	0.42	60.02	0.14	0.11	62.74
	x5	1.07	1.25	1527.90	1.12	0.99	740.88
Calibration Phase	x1	0.00	0.00	0.02	0.06	0.01	2.06
	x5	0.00	0.00	0.09	0.28	0.08	3.33
Testing Phase	x1	0.35	0.41	0.36	0.39	0.36	0.37
	x5	1.83	1.89	1.90	1.90	1.79	1.87

Note: The time of data collection is excluded.

Since the calibration sample set is small in this experiment, using more calibration samples generally provides useful information on learning the data distribution after electrode shift, i.e., a model with more calibration samples is more accurate. The results also show that additional calibration samples improve more to CA and DA than our method because the calibration samples for CA and DA contain labels, which provides more information than ones used in our method. It also explains why the accuracy of our model increases more slowly than CA and DA with the increase of the number of calibration samples.

3) Running Time: The running times of the training, calibration, and test phases of the methods are investigated by using different sizes of datasets, and the results are given in Table VII. Xi denotes our original dataset is duplicated i times with dummy samples in order to evaluate the influence of the sample number on the running time of the methods. In x1, the training, calibration, and test sets contain 27 900, 500, and 1700 samples, respectively.

It should be noted that the data collection time is not counted in any phase in this investigation since it highly depends on the system design, which is not covered in this study. In practice, it is expected that the training data collection time of our method and DA is longer than others since a number of datasets with different electrode shifts are required. The test data collection times of all methods are the same since the requirement on a test sample is the same. Moreover, the calibration data collection of our method is less time-consuming than other calibration methods since a subject only needs to do the preselected motions arbitrarily as opposed to all motion classes following a strict order.

The training phase includes LDA training, and the preparation time of any components required by a model. The running times of *base*, DA, and SE are almost the same in the training phase since they only require the training of LDAs. However, the searching on a common space among different training sets in gCMCA and training of the parameter estimators in our method increase the training time. The training time of these methods increases linearly with the increase of sample number. However, CA has the longest training time among all methods since calibration and SE are required for each training dataset with different electrode shifts, and the time grows quadratically with the size of the training set.

The calibration time of CA and SE grows slowly with the increase of the calibration samples number since the parameters of LDA are recalculated according to the newly collected samples. Although our method requires the longest calibration time due to the clustering process, benchmark class identification, and parameter estimation, the time is still reasonable in practical use. Moreover, our collection time of the calibration data, which is not considered in this comparison, should be significantly shorter than other traditional recalibration methods since no restrictive rule is required. As a result, the calibration time of our method may not necessarily be longer than other methods. All methods have similar running times used for classifying a sample on average.

V. Conclusion

Calibration plays an important role in reducing the influence of electrode shift on sEMG-based hand gesture recognition. However, most calibration methods require labeled samples of all motions that are time-consuming and inconvenient to collect, since electrode shift may happen several times each day. Although some methods do not rely on a calibration set, they only perform well for slight electrode shift, i.e., the sample distribution does change too much. This article proposes an unsupervised domain adaptation method that simplifies the calibration data collection process, in which a user is only required to perform the benchmark motions in an arbitrary order. The sample distributions changed by electrode shift are then estimated according to the unlabeled benchmark motion samples. Our method significantly reduces the effort of data collection and provides a user friendly data collection process compared with the existing ones, which require labeled samples of all motions under rigid instructions.

The experimental results on our collected dataset suggest that our method achieves higher accuracy than methods without calibration (*base* and gCMCA), and the methods with calibration using unlabeled samples (SE). In comparison with methods calibrating with labeled samples (i.e., CA and DA), the accuracy of our method is lower, as we sacrifice some accuracy for user convenience. Our method is more convenient to users as no label information is required after electrode shift, and only a subset of total motion classes are required. Moreover, the difference in accuracy between our method, and CA and DA reduces when the influence of electrode shift is small.

The difficulty of the mean and covariance estimation increases when the number of classes increases and the classes are closer together, i.e., two gestures are similar. One future work may focus on the improvement of the parameter estimation by using a more advanced prediction method, e.g., deep learning. However, the time complexity of the prediction model should also be considered. Moreover, our study indicates that using more historical data affected by electrode shift improves the performance of our method. However, data collection is time-consuming and expensive. One possible solution to the high cost of data collection is to reuse the knowledge extracted from the data of other subjects.

References

[1] X. Yang, J. Yan, and H. Liu, “Comparative analysis of wearable a-mode ultrasound and sEMG for muscle-computer interface,” *IEEE Trans. Biomed. Eng.*, vol. 67, no. 9, pp. 2434–2442, Sep. 2020.

[2] M. A. Simão, N. Mendes, O. Gibaru, and P. Neto, “A review on electromyography decoding and pattern recognition for human-machine interaction,” *IEEE Access*, vol. 7, pp. 39564–39582, 2019.

[3] Y. Fang, D. Zhou, K. Li, Z. Ju, and H. Liu, “Attribute-driven granular model for EMG-based pinch and fingertip force grand recognition,” *IEEE Trans. Cybern.*, vol. 51, no. 2, pp. 789–800, Feb. 2021.

[4] S. Kanoga, A. Kanemura, and H. Asoh, “Are armband semg devices dense enough for long-term use?—Sensor placement shifts cause significant reduction in recognition accuracy,” *Biomed. Signal Process. Control*, vol. 60, 2020, Art. no. 101981.

[5] Z. Li, X. Zhao, G. Liu, B. Zhang, D. Zhang, and J. Han, “Electrode shifts estimation and adaptive correction for improving robustness of sEMG-based recognition,” *IEEE J. Biomed. Health Informat.*, vol. 25, no. 4, pp. 1101–1110, Apr. 2021.

[6] Q. Ding, X. Zhao, J. Han, C. Bu, and C. Wu, “Adaptive hybrid classifier for myoelectric pattern recognition against the interferences of outlier motion, muscle fatigue, and electrode doffing,” *IEEE Trans. Neural Syst. Rehabil. Eng.*, vol. 27, no. 5, pp. 1071–1080, May 2019.

[7] D. Farina *et al.*, “The extraction of neural information from the surface EMG for the control of upper-limb prostheses: Emerging avenues and challenges,” *IEEE Trans. Neural Syst. Rehabil. Eng.*, vol. 22, no. 4, pp. 797–809, Jul. 2014.

[8] J. L. Betthauser *et al.*, “Limb position tolerant pattern recognition for myoelectric prosthesis control with adaptive sparse representations from extreme learning,” *IEEE Trans. Biomed. Eng.*, vol. 65, no. 4, pp. 770–778, Apr. 2018.

[9] Z. Fan, Z. Wang, G. Li, and R. Wang, “A canonical correlation analysis based EMG classification algorithm for eliminating electrode shift effect,” in *Proc. IEEE 38th Annu. Int. Conf. Eng. Med. Biol. Soc.*, 2016, pp. 867–870.

[10] J. M. Hahne, M. A. Schweisfurth, M. Koppe, and D. Farina, “Simultaneous control of multiple functions of bionic hand prostheses: Performance and robustness in end users,” *Sci. Robot.*, vol. 3, no. 19, 2018, Art. no. eaat3630.

[11] J. L. Betthauser, L. E. Osborn, R. R. Kaliki, and N. V. Thakor, “Electrode-shift tolerant myoelectric movement-pattern classification using extreme learning for adaptive sparse representations,” in *Proc. IEEE Biomed. Circuits Syst. Conf.*, 2017, pp. 1–4.

[12] J. He and X. Zhu, “Combining improved gray-level co-occurrence matrix with high density grid for myoelectric control robustness to electrode shift,” *IEEE Trans. Neural Syst. Rehabil. Eng.*, vol. 25, no. 9, pp. 1539–1548, Sep. 2017.

[13] H. Daley, K. Englehart, L. Hargrove, and U. Kuruganti, “High density electromyography data of normally limbed and transradial amputee subjects for multifunction prosthetic control,” *J. Electromyogr. Kinesiol.*, vol. 22, no. 3, pp. 478–484. 2012.

[14] A. Stango, F. Negro, and D. Farina, “Spatial correlation of high density EMG signals provides features robust to electrode number and shift in pattern recognition for myocontrol,” *IEEE Trans. Neural Syst. Rehabil. Eng.*, vol. 23, no. 2, pp. 189–198, Mar. 2015.

[15] B. Lv, X. Sheng, and X. Zhu, “Improving myoelectric pattern recognition robustness to electrode shift by autoencoder,” in *Proc. 40th Annu. Int. Conf. IEEE Eng. Med. Biol. Soc.*, 2018, pp. 5652–5655.

[16] X. Zhang, L. Wu, B. Yu, X. Chen, and X. Chen, “Adaptive calibration of electrode array shifts enables robust myoelectric control,” *IEEE Trans. Biomed. Eng.*, vol. 67, no. 7, pp. 1947–1957, Jul. 2020.

[17] J. Liu, X. Sheng, D. Zhang, and X. Zhu, “Boosting training for myoelectric pattern recognition using mixed-LDA,” in *Proc. 36th Annu. Int. Conf. IEEE Eng. Med. Biol. Soc.*, 2014, pp. 14–17.

[18] J. Liu, X. Sheng, D. Zhang, J. He, and X. Zhu, “Reduced daily recalibration of myoelectric prosthesis classifiers based on domain adaptation,” *IEEE J. Biomed. Health Informat.*, vol. 20, no. 1, pp. 166–176, Jan. 2016.

[19] M. M.-C. Vidovic, H.-J. Hwang, S. Amsüss, J. M. Hahne, D. Farina, and K.-R. Müller, “Improving the robustness of myoelectric pattern recognition for upper limb prostheses by covariate shift adaptation,” *IEEE Trans. Neural Syst. Rehabil. Eng.*, vol. 24, no. 9, pp. 961–970, Sep. 2016.

[20] X. Zhu, J. Liu, D. Zhang, X. Sheng, and N. Jiang, “Cascaded adaptation framework for fast calibration of myoelectric control,” *IEEE Trans. Neural Syst. Rehabil. Eng.*, vol. 25, no. 3, pp. 254–264, Mar. 2017.

[21] X. Chen, D. Zhang, and X. Zhu, “Application of a self-enhancing classification method to electromyography pattern recognition for multifunctional prosthesis control,” *J. Neuroengineering Rehabil.*, vol. 10, no. 1, 2013, Art. no. 44.

[22] U. Côté-Allard *et al.*, “Unsupervised domain adversarial self-calibration for electromyography-based gesture recognition,” *IEEE Access*, vol. 8, pp. 177941–177955, 2020.

[23] J. Liu, X. Sheng, D. Zhang, N. Jiang, and X. Zhu, “Towards zero retraining for myoelectric control based on common model component analysis,” *IEEE Trans. Neural Syst. Rehabil. Eng.*, vol. 24, no. 4, pp. 444–454, Apr, 2016.

[24] F. Duan, X. Ren, and Y. Yang, “A gesture recognition system based on time domain features and linear discriminant analysis,” *IEEE Trans. Cogn. Devel. Syst.*, vol. 13, no. 1, pp. 200–208, Mar. 2021.

[25] F. S. Botros, A. Phinyomark, and E. J. Scheme, “Electromyography-based gesture recognition: Is it time to change focus from the forearm to the wrist?,” *IEEE Trans. Ind. Informat.*, vol. 18, no. 1, pp. 174–184, Jan. 2022.

[26] Y. Fang, H. Liu, G. Li, and X. Zhu, “A multichannel surface EMG system for hand motion recognition,” *Int. J. Humanoid Robot.*, vol. 12, no. 02, 2015, Art. no. 1550011.

[27] Y. Fang, X. Zhu, and H. Liu, “Development of a surface EMG acquisition system with novel electrodes configuration and signal representation,” in *Proc. Int. Conf. Intell. Robot. Appl.*, vol. 8102, 2013, pp. 405–414.

[28] C. P. Robinson, B. Li, Q. Meng, and M. T. Pain, “Pattern classification of hand movements using time domain features of electromyography,” in *Proc. 4th Int. Conf. Movement Comput.*, 2017, pp. 1–6.

[29] A. Liaw *et al.*, “Classification and regression by randomforest,” *R News*, vol. 2, no. 3, pp. 18–22, 2002.

[30] R. Couronné, P. Probst, and A.-L. Boulesteix, “Random forest versus logistic regression: A large-scale benchmark experiment,” *BMC Bioinf.*, vol. 19, no. 1, 2018, Art. no. 270.